SSRG International Journal of Mechanical Engineering
ISSN: 2348-8360/ https://doi.org/10.14445/23488360/IJME-V13I1P105

Volume 13 Issue 1, 55-60, January 2026


*Original Article*

# Fabrication and Microstructural Study of Pressure-Assisted Nano-Silver Lap-Shear Joints for Power Electronics Packaging

Phuoc-Thanh Tran[1], Quang-Bang Tao[1*], Van-Trung Pham[1]

[1]*Department of Mechanical Engineering, University of Science and Technology, The University of Danang, Danang city, Viet Nam.*

**Corresponding Author : tqbang@dut.udn.vn*

Received: 05 November 2025 Revised: 07 December 2025 Accepted: 05 January 2026 Published: 14 January 2026

***Abstract*** *- High-temperature power electronics place demanding requirements on interconnect reliability, yet most existing reports focus on either pressure or bondline thickness when evaluating nano-silver joints. Systematic data combining both factors, particularly in a controlled lap-shear configuration, remains limited. In this work, nano-silver joints were fabricated using a laboratory-built sintering stage capable of independent control of temperature (±3 °C), pressure (±0.05 MPa), and bondline spacing (±3 µm). A commercial nano-Ag paste was sintered at 280 °C under pressures of 1.0–1.5 MPa with target bondline thicknesses of 50, 70, and 100 µm. SEM observations showed continuous neck formation, uniform particle coalescence, and no visible cracking at the Ag–Cu interface. To verify that the joints were mechanically sound before entering a larger study, several preliminary lap-shear tests were performed using a custom shear fixture with high-resolution load and displacement measurement. Under quasi-static loading (strain rate ~ $1\times10^{-4}$ $s^{-1}$, 25 °C), the joints produced strengths in the range of approximately 15–28 MPa depending on pressure and thickness, consistent with expected values for early-stage sintered Ag layers. These results confirm that the custom sintering setup can repeatedly produce well-bonded joints with stable morphology and predictable mechanical response, providing a reliable basis for subsequent detailed mechanical characterization. This work is among the few studies that simultaneously regulate temperature, pressure, and bondline thickness in a controlled lap-shear configuration.*

***Keywords*** *- Nano-silver sintering, Lap-shear joints, Bondline thickness control, Pressure-assisted fabrication, High-temperature interconnects, Microstructural characterization.*

## 1. Introduction

Power electronic converters increasingly operate at elevated junction temperatures, often 250–300 °C in traction, aerospace, and renewable-energy systems. Under these conditions, the bonding interface becomes a major reliability concern. Joint degradation can adversely influence both electrical behavior and overall service life. Conventional Sn-Pb and Sn-Ag-Cu solders remain widely used due to established processing routes.

However, their creep resistance and melting-temperature limits restrict operation above ~250 °C. Pb-based alloys also face regulatory constraints, whereas Au-based systems offer excellent stability but are economically impractical [1–5]. Alternative approaches—such as transient-liquid-phase bonding and Cu sintering—show promise but can suffer from interfacial reactions, void formation, or long processing cycles [6–10].

Sintered nano-silver has therefore emerged as a strong candidate for high-temperature die-attach because it forms metallurgical bonds below 300 °C while providing high conductivity and good creep resistance for SiC and GaN power devices [11–15]. Earlier studies have described dense microstructures, stable oxidation behavior, and durable Ag–Cu interfaces. While most studies concentrate on thin die-attach layers, mechanically relevant joint geometries—such as lap-shear configurations—have received much less attention. Previous studies indicate that factors such as pressure, thickness, or strain rate can influence the shear or fatigue performance of nano-silver joints [19–23]. Many studies, however, omit essential conditions—such as pressure uniformity or heating profiles—which makes direct comparison difficult.

A further limitation relates to process reproducibility. Recent reviews have summarized progress in areas such as

paste formulation and sintering behavior. Even so, reliable fabrication procedures that control temperature, pressure, and joint thickness remain largely unstandardized for mechanically loaded joints [16–20]. Although tools such as real-time sensing and IoT-based logging can improve process stability and traceability, they are rarely included in laboratory-scale sintering systems.

The present work addresses these gaps by developing a controlled pressure-assisted nano-silver sintering process tailored for lap-shear joints. A custom fabrication tool with independent control of temperature, pressure, and bondline spacing—augmented by real-time monitoring—was implemented to improve process consistency. Resulting joints were examined by SEM to assess densification, porosity, and interface quality. Our objective is to develop a reproducible fabrication route that yields nano-silver joints appropriate for later mechanical evaluation and high-temperature applications.

## 2. Materials and Methods

### *2.1. Materials*

Commercial NanoTach® nano-silver paste (NBE Technologies, Singapore) was used as the joining material. The paste contains approximately 85 ± 2 wt% silver nanoparticles dispersed in an organic binder–solvent matrix and is formulated for high-temperature power electronics applications. Particle sizes fall in the 50–100 nm range, as previously reported in the datasheet and verified by TEM/DLS measurements in earlier work.

The paste includes several functional components: silver nanoparticles as the conductive phase; organic binders that provide green strength and control rheology; and a mixture of low-boiling solvents and thixotropic additives that assist in deposition and evaporation. Small quantities of stabilizers are added to maintain dispersion and prevent particle agglomeration. A summary of the typical composition is provided in Table 1 [28].

Copper substrates (99.9 % purity) were selected due to their common use in power-module packaging and their compatibility with silver. Prior to bonding, the substrates were mechanically polished and gold-plated to limit surface oxidation and ensure a clean interface during sintering. The same pretreatment protocol has been used widely in high-reliability die-attach studies and was retained here for consistency.

**Table 1. Typical composition and functional roles of constituents in the NanoTach® nano-silver paste used for lap-shear joint fabrication**

| Component | Typical content (wt%) | Function |
|---|---|---|
| Silver nanoparticles | ~85 % | Provide electrical/thermal conductivity; form metallurgical bonds via sintering. |
| Organic binders | ~10–20 % | Ensure adhesion, control rheology, and maintain paste integrity before sintering. |
| Low-boiling solvents & thixotropic agents | <10 % | Adjust fluidity, aid solvent evaporation. |
| Stabilizing / adhesion additives | <5 % | Prevent agglomeration, improve storage stability. |

### *2.2. Sintering System*

A custom-built sintering system was used to fabricate the nano-silver lap-shear joints. The setup consists of a rigid frame supporting a modular heating and pressing unit designed for controlled laboratory bonding. Temperature regulation is handled by a PID controller coupled with a type-K thermocouple, allowing the programmed thermal profile to be followed with an accuracy of about ±3 °C. A ceramic resistance heater surrounds the bonding region and helps maintain a relatively uniform temperature across the joint area.

Pressure is applied through a pneumatic actuator integrated with a Z-type load cell. Real-time feedback enables closed-loop adjustment, keeping the applied pressure within approximately ±0.05 MPa during the sintering cycle. We found that keeping the pressure within ±0.05 MPa prevented the small voids sometimes seen in earlier test runs. Bondline thickness is maintained using a fixed spacer–die assembly, giving a practical tolerance of roughly ±3 µm across specimens.

Sensors for temperature, pressure, and cycle timing are connected to an IoT-based logging module that records all stages of the process. These data allow verification of system stability and provide traceable records for each run. In practice, the combination of closed-loop control and continuous logging makes it straightforward to identify deviations and adjust operating conditions between batches. The system also enables heating and pressing components to be reconfigured for different specimen geometries, which has been useful when testing joints of varying sizes or thickness targets. Major components of the setup are shown in Figure 1. Before starting the main experiments, we checked the system with several runs. The temperature and pressure curves were close to the programmed profiles, so we used the setup for the microstructural study.


**Fig. 1 Schematic of the custom nano-silver sintering system showing the heating module, pneumatic loading assembly, and sensor–control unit. The setup includes the mold and heater block, insulation stack, pneumatic regulator with load-cell feedback, and the temperature/force displays used for process monitoring. The arrangement provides controlled temperature–pressure application and stable bondline alignment during sintering**

## *2.3. Fabrication Procedure for Single Lap-Shear Specimens*

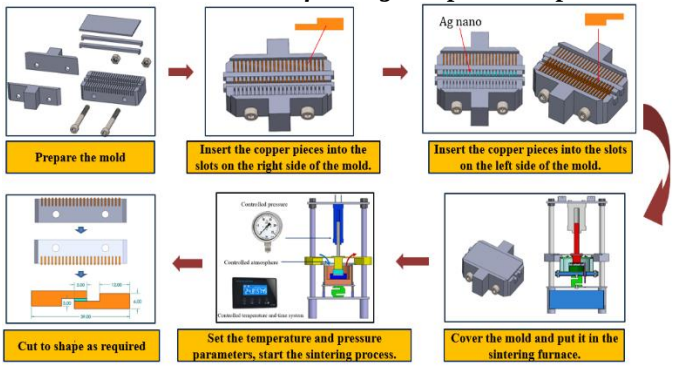


**Fig. 2 Workflow for fabricating pressure-assisted nano-silver lap-shear joints, including surface preparation, mold assembly, sintering, and post-bonding inspection**

The fabrication of nano-silver lap-shear joints followed a standardized five-step workflow to ensure consistent bondline geometry and joint quality. The fabrication sequence followed the five steps described below.

### *2.3.1. Step 1: Preparation of Equipment and Materials*

The sintering system was powered on and checked to confirm stable operation of the heater, pneumatic actuator, pressure sensor, and logging interface. NanoTach® nano-silver paste was selected as the bonding material, and copper substrates were cleaned to remove surface contaminants.

### *2.3.2. Step 2: Surface Pretreatment*

Mold components were ultrasonically cleaned in acetone. Copper substrates were mechanically polished and gold-plated to minimize oxidation and provide a clean interface for bonding. This pretreatment approach is consistent with established die-attach practice.

### *2.3.3. Step 3: Mold Assembly*

The substrates were positioned in a precision alignment fixture designed to maintain parallelism and a defined overlap region. Nano-silver paste was applied uniformly to the bonding area, and the spacer–die assembly was used to set the nominal bondline thickness. The assembled mold was then placed inside the sintering chamber.

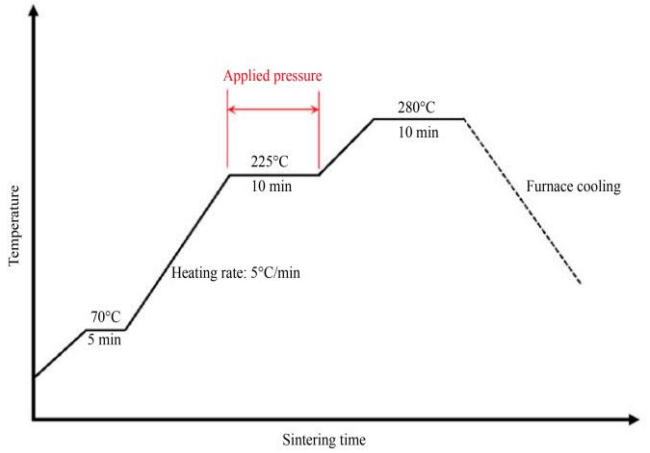


**Fig. 3 Thermal and pressure profile for the nano-silver sintering process, showing heating, holding, and cooling stages under a reducing $H_2/N_2$ atmosphere**

### *2.3.4. Step 4: Sintering Process*

The programmed thermal–pressure cycle consisted of three phases, as illustrated in Figure 3.

*Heating Phase*

The joint was brought from room temperature to the target sintering temperature under controlled ramping while a preset preload was applied.

*Holding Phase*

Temperature and pressure were maintained within their control tolerances to promote solvent evaporation, particle rearrangement, and neck growth. System logging recorded temperature, pressure, and time continuously throughout this stage.

*Cooling Phase*

The joint was cooled under a reduced load to stabilize the microstructure and avoid thermal shock before removal. These phases were executed automatically by the controller, with real-time monitoring to verify profile stability for each run.

### *2.3.5. Step 5: Post-Sintering Evaluation*

After cooling, the mold was disassembled, and the bonded specimens were removed. Basic handling checks were performed to screen for gross defects. Optical microscopy and SEM were then used to verify bondline integrity, assess thickness uniformity, and examine the morphology of the sintered layer.

## 3. Results and Discussion

### *3.1. Sintered Nano-Silver Joint Specimen*

Lap-shear joints were successfully fabricated using the pressure-assisted nano-silver sintering procedure described in Section 2.3. All specimens were processed within the designated temperature–pressure window of 280 °C and 1.0–1.5 MPa, with nominal bondline thicknesses of 50, 70, and 100 µm. Across several fabrication batches, the measured bondline thicknesses stayed within ±3 µm of the targets, suggesting that the setup provided reasonably consistent control. Depth-gauge measurements taken at three locations on each specimen showed only minor variation, typically not exceeding 2–4 µm.

During visual inspection, the copper substrates showed proper alignment after sintering, with no noticeable warpage or lateral shift. The sintered silver layers appeared continuous and well-shaped without macro-scale cracks or delamination. Slight deviations in thickness were occasionally observed, likely due to minor surface unevenness and manual paste spreading. This variation remains within the accepted ±5 µm tolerance commonly used for high-reliability interconnects.

Basic handling checks were performed right after demolding to assess joint integrity. None of the samples showed edge lifting or cohesive failure under gentle bending or fingertip shear, indicating that the joints had achieved sufficient densification and adhesion. This informal check was performed for each fabrication batch (typically 3–4 samples per batch) and consistently showed intact joints before formal shear testing.

Cross-sectional checks confirmed that the fixture and spacers effectively controlled the bondline geometry. Observed layer thicknesses for the 50-, 70-, and 100-µm groups aligned with the expected consolidation trend noted earlier: higher pressure (1.5 MPa) produced slightly thinner layers than 1.0 MPa. These consistent geometries reduce stress concentration effects and support reliable microstructural comparisons among specimens.

In general, the fabricated joints exhibited uniform layer geometry, stable adhesion, and clean Ag–Cu interfaces. After adjusting the pressure feedback in the early tests, the system produced joints with consistent geometry. These batches were adequate for proceeding to microstructural and mechanical examination.

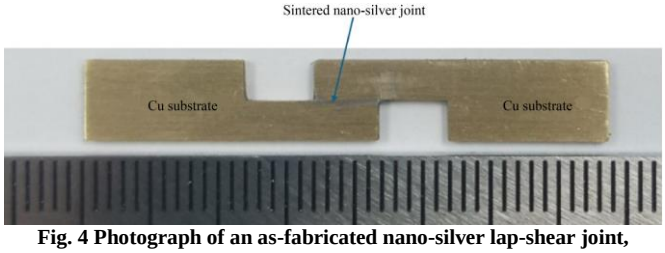


**Fig. 4 Photograph of an as-fabricated nano-silver lap-shear joint, demonstrating uniform alignment and stable bondline geometry**

### *3.2. Microstructural Analysis*

Cross-sectional SEM imaging was performed to evaluate the internal morphology of the sintered nano-silver bondlines. A JEOL JSM-IT210LA operated at 10–15 kV in SE mode was used for all observations. Each specimen was examined at three representative regions along the overlap to confirm that the microstructure was consistent across the joint. Representative images at different magnifications are shown in Figure 5.

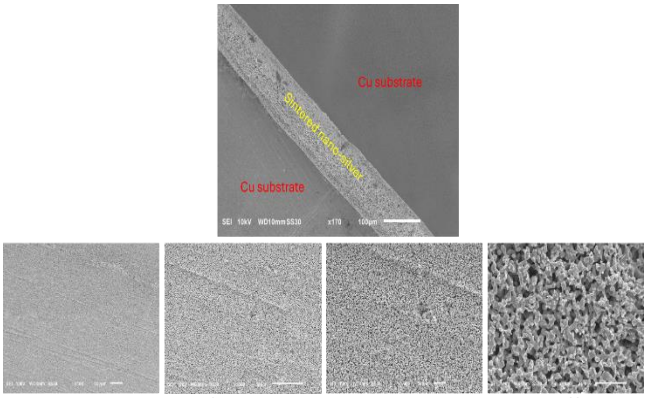


**Fig. 5 SEM images of the sintered nano-silver bondline at different magnifications, showing dense particle packing, uniform neck growth, and a clean Ag–Cu interface**

Low-magnification images showed a generally dense and uniform bondline without obvious large defects or unbonded regions. The Ag particles retained their expected nanoscale morphology, with characteristic diameters in the 40–80 nm range. The relatively narrow size distribution suggests that the paste retained good stability during deposition and the initial solvent-removal stage. From the images, the particle distribution appeared uniform, which likely contributed to the similar densification we observed across samples.

Pores were present but generally small and rounded. Image-based estimation performed on several fields of view gave a porosity level of approximately 14 %, with variations of less than ±1 % between inspected regions. The measured porosity aligns with values reported for pressure-assisted nano-silver bonding and should not affect structural integrity at this scale. A uniform pore distribution reduces local stress concentrations, a factor that generally improves the performance of joints under mechanical loading.

Higher-magnification images revealed continuous neck formation between adjacent Ag particles, creating a coherent metallic network. Neck radii increased notably compared with the as-deposited paste, confirming that sufficient diffusion occurred during the holding stage of the thermal cycle. Grain sizes were estimated in the 200–250 nm range based on multiple line-profile measurements. This grain size is consistent with reports of nano-silver sintered at similar temperatures and provides a microstructural basis for the stable handling strength observed in Section 3.1.

Across the inspected regions, the Ag–Cu interface remained continuous. No cracking, voiding, or separation was detected at the interface, and the contrast transition between Ag and Cu suggests limited interdiffusion rather than abrupt mechanical contact. This interfacial condition aligns with expectations for sintering at 280 °C under applied pressure and indicates that the fixture maintained adequate alignment and contact throughout the bonding process.

In contrast to Sn-based solders, our samples did not show thick intermetallic layers at the Cu interface. This difference may influence shear behavior at higher temperatures, although confirming this would require additional testing. Conventional solders often develop coarser grains and thicker intermetallic layers at the Cu interface, which can compromise shear performance at elevated temperatures. In contrast, the fine Ag neck network and stable Ag–Cu interface observed here indicate better thermal stability and reduced susceptibility to interfacial degradation. Although a full mechanical comparison lies beyond the scope of this work, these characteristics are consistent with the superior high-temperature reliability commonly reported for sintered silver materials.

Based on the SEM images, the joints showed relatively uniform particle packing and a continuous Ag–Cu interface. The porosity was around 14 %, consistent across regions. The combination of consistent particle coalescence, stable interface quality, and the absence of macroscopic defects indicates that the sintering setup provided good process control. These findings support the suitability of the fabricated joints for subsequent mechanical testing and long-term reliability evaluation.

## 4. Conclusion

This study developed and validated a pressure-assisted nano-silver sintering procedure that can produce lap-shear joints with controlled and repeatable bondline geometry. With regulated temperature–pressure conditions (280 °C, 1.0–1.5 MPa) and a guided alignment fixture, joints with nominal thicknesses of 50–90 μm were produced with small thickness variation and consistently aligned substrates across batches.

Microstructural observations showed dense particle packing, continuous neck formation, and intact Ag–Cu interfaces without evidence of cracking or delamination. The uniformly distributed porosity of approximately 14 % further suggests a well-connected metallic network that is expected to support stable shear performance. Overall, the joints showed the key microstructural characteristics that are generally associated with reliable mechanical behavior in pressure-assisted nano-silver systems.

Our experiments showed that the system maintained the target joint thickness within a narrow range. The microstructural results were also consistent across samples, which allowed us to use the setup for further mechanical studies. A full analysis of shear behavior was beyond the scope of this study, but the current results highlight the need for future work that links processing parameters with microstructural evolution and mechanical response.

## Funding Statement

This research is funded by the Fund of Fujikin, code number of Project: T2023FSF-02-02.

## References

[1] Norliza Ismail et al., “A Review of Extreme Condition Effects on Solder Joint Reliability: Understanding Failure Mechanisms,” *Defence Technology*, vol. 41, pp. 134-158, 2024. [CrossRef] [Google Scholar] [Publisher Link]

[2] M. Lederer, A. Betzwar Kotas, and G. Khatibi, “A Lifetime Assessment and Prediction Method for Large Area Solder Joints,” *Microelectronics Reliability*, vol. 114, pp. 1-7, 2020. [CrossRef] [Google Scholar] [Publisher Link]

[3] Qilong Guan et al., “Research Progress on the Solder Joint Reliability of Electronics Using in Deep Space Exploration,” *Chinese Journal of Mechanical Engineering*, vol. 36, no. 1, pp. 1-13, 2023. [CrossRef] [Google Scholar] [Publisher Link]

[4] Kathlene N. Reeve et al., “Advances in Pb-Free Solder Microstructure Control and Interconnect Design,” *Journal of Phase Equilibria and Diffusion*, vol. 37, no. 4, pp. 369-386, 2016. [CrossRef] [Google Scholar] [Publisher Link]

[5] R. Darveaux, “Effect of Simulation Methodology on Solder Joint Crack Growth Correlation,” *2000 Proceedings. 50th Electronic Components and Technology Conference (Cat. No.00CH37070)*, Las Vegas, NV, USA, pp. 1048-1058, 2000. [CrossRef] [Google Scholar] [Publisher Link]

[6] Hyejun Kang, Ashutosh Sharma, and Jae Pil Jung, “Recent Progress in Transient Liquid Phase and Wire Bonding Technologies for Power Electronics,” *Metals*, vol. 10, no. 7, pp. 1-21, 2020. [CrossRef] [Google Scholar] [Publisher Link]

[7] Omid Mokhtari, “A review: Formation of Voids in Solder Joint During the Transient Liquid Phase Bonding Process - Causes and Solutions,” *Microelectronics Reliability*, vol. 98, pp. 95-105, 2019. [CrossRef] [Google Scholar] [Publisher Link]

[8] Junhyuk Son et al., “Thermal Reliability of Cu Sintering Joints for High-Temperature Die Attach,” *Microelectronics Reliability*, vol. 147, 2023. [CrossRef] [Google Scholar] [Publisher Link]

[9] He Diao et al., “Study on the Interfacial Reactions for Ag/Sn/Cu TLP During Transient Liquid Phase Soldering Process,” *Journal of Materials Science: Materials in Electronics*, vol. 36, no. 5, 2025. [CrossRef] [Google Scholar] [Publisher Link]

[10] H. Zhang, and K. Suganuma, *Sintered Silver for LED Applications*, Die-Attach Materials for High Temperature Applications in Microelectronics Packaging, Springer, Cham, pp. 35-65, 2019. [CrossRef] [Google Scholar] [Publisher Link]
[11] Zhongqing Zhang et al., "Research on Sintering Process and Thermal Conductivity of Hybrid Nanosilver Solder Paste based on Molecular Dynamics Simulation," *Microelectronics Reliability*, vol. 126, 2021. [CrossRef] [Google Scholar] [Publisher Link]
[12] Hongqiang Zhang et al., "Microstructural and Mechanical Evolution of Silver Sintering Die Attach for Sic Power Devices During High Temperature Applications," *Journal of Alloys and Compounds*, vol. 774, pp. 487-494, 2019. [CrossRef] [Google Scholar] [Publisher Link]
[13] Yansong Tan, Xin Li, and Xu Chen, "Fatigue and Dwell-Fatigue Behavior of Nano-Silver Sintered Lap-Shear Joint at Elevated Temperature," *Microelectronics Reliability*, vol. 54, no. 3, pp. 648-653, 2014. [CrossRef] [Google Scholar] [Publisher Link]
[14] Hyeong-Woo Kang, and Jae Pil Jung, "Recent Sinter-Bonding Technology of Power Semiconductor Using Silver Particles," *Journal of Welding and Joining*, vol. 43, no. 2, pp. 119-127, 2025. [CrossRef] [Google Scholar] [Publisher Link]
[15] Keisuke Wakamoto, and Takahiro Namazu, "Mechanical Characterization of Sintered Silver Materials for Power Device Packaging: A Review," *Energies*, vol. 17, no. 16, pp. 1-22, 2024. [CrossRef] [Google Scholar] [Publisher Link]
[16] Chuantong Chen et al., "Development of SiC Power Module Structure by Micron-Sized Ag-Paste Sinter Joining on Both Die and Heatsink to Low-Thermal-Resistance and Superior Power Cycling Reliability," *IEEE Transactions on Power Electronics*, vol. 39, no. 9, pp. 10638-10648, 2024. [CrossRef] [Google Scholar] [Publisher Link]
[17] Meiyu Wang et al., "Characterization of Multiple Commercial Sintered-Silver Pastes as Die Attachment for Power Electronics Packaging: Materials, Processing, and Properties," *IEEE Journal of Emerging and Selected Topics in Power Electronics*, vol. 13, no. 1, pp. 892-903, 2025. [CrossRef] [Google Scholar] [Publisher Link]
[18] R. Khazaka, L. Mendizabal, and D. Henry, "Review on Joint Shear Strength of Nano-Silver Paste and its Long-Term High-Temperature Reliability," *Journal of Electronic Materials*, vol. 43, no. 7, pp. 2459-2466, 2014. [CrossRef] [Google Scholar] [Publisher Link]
[19] Lihua Gao et al., "Microstructure and Bonding Strength of Low-Temperature Sintered Ag/Nano-Ag Films/Ag Joints," *Metals*, vol. 13, no. 11, pp. 1-12, 2023. [CrossRef] [Google Scholar] [Publisher Link]
[20] Cheng Qian et al., "Tensile Characterization and Constitutive Modeling of Sintered Nano-Silver Particles Over a Range of Strain Rates and Temperatures," *Microelectronics Reliability*, vol. 132, 2022. [CrossRef] [Google Scholar] [Publisher Link]
[21] Jens Heilmann et al., "Physics of Failure based Lifetime Modelling for Sintered Silver Die Attach in Power Electronics: Accelerated Stress Testing by Isothermal Bending and Thermal Shock in Comparison," *Microelectronics Reliability*, vol. 145, 2023. [CrossRef] [Google Scholar] [Publisher Link]
[22] Rosidah Alias, and Sabrina Mohd Shapee, *Rheological Behaviors and Their Correlation with Printing Performance of Silver Paste for LTCC Tape*, Rheology, IntechOpen, 2012. [CrossRef] [Google Scholar] [Publisher Link]
[23] Kun Ma et al., "A Micromechanical Analysis to the Viscoplastic Behavior of Sintered Silver Joints under Shear Loading," *Materials*, vol. 16, no. 12, pp. 1-15, 2023. [CrossRef] [Google Scholar] [Publisher Link]
[24] Wei Liu et al., "Recent Progress in Rapid Sintering of Nanosilver for Electronics Applications," *Micromachines*, vol. 9, no. 7, pp. 1-17, 2018. [CrossRef] [Google Scholar] [Publisher Link]
[25] Yujun Gao et al., "Effects of Organic Vehicle on the Rheological and Screen-Printing Characteristics of Silver Paste for LTCC Thick Film Electrodes," *Materials*, vol. 15, no. 5, pp. 1-11, 2022. [CrossRef] [Google Scholar] [Publisher Link]
[26] Hui Yang, and Jihui Wu, "Improvement of Sintering Performance of Nanosilver Paste by Tin Doping," *Journal of Nanomaterials*, vol. 2020, pp. 1-6, 2020. [CrossRef] [Google Scholar] [Publisher Link]
[27] Najwa Ibrahim, John O. Akindoyo, and M. Mariatti, "Recent Development in Silver-based Ink for Flexible Electronics," *Journal of Science: Advanced Materials and Devices*, vol. 7, no. 1, pp. 1-13, 2022. [CrossRef] [Google Scholar] [Publisher Link]
[28] NanoTach® Die-Attach Products, NBE Technologies LLC. [Online]. Available: https://www.nbetech.com/products